Acoust. Sci. & Tech. **31**, 1 (2010)

PAPER

Efficiency of edge-modified noise barriers: Intrinsic efficiency determination of practical products and prediction of the diffracted sound field

Tomonao Okubo[1,*], Toshio Matsumoto[1], Kohei Yamamoto[1], Osamu Funahashi[2] and Kunio Nakasaki[2]

[1]*Kobayasi Institute of Physical Research, 3–20–41 Higashi-motomachi, Kokubunji, Tokyo, 185–0022 Japan*
[2]*Nippon Expressway Research Institute Co. Ltd., 1–4–1 Tadao, Machida, Tokyo, 194–8508 Japan*

(*Received 30 March 2009, Accepted for publication 7 September 2009*)

Abstract: In this paper, the noise shielding efficiency of barriers with an acoustic device mounted on their top edge for reducing sound diffraction is described. The authors have already found that the intrinsic efficiency of the device, which is related to the noise-reducing mechanisms, is a function of the angles of the source and receiver but independent of their radii. In the present paper, a novel procedure based on the previous finding is applied to determine the acoustical efficiencies of practical edge-modifying products in the near field, and the results are utilized in calculations to predict sound diffraction behind the edge-modified barriers in the far field. It is proved that the novel method provides an accurate prediction.

Keywords: Noise barriers, Diffraction, Sound propagation, Road traffic noise

PACS number: 43.50.Gf [doi:10.1250/ast.31.56]

1. INTRODUCTION

Barriers are commonly applied to reduce noise from road traffic. After the invention of an absorbing cylindrical edge by Fujiwara and Ono [1], the noise-shielding efficiency of barriers can be improved when their top edge is appropriately modified to reduce diffraction. In this paper, barriers with acoustical devices on their top edge to reduce diffraction are referred to as edge-modified barriers. Approximately twenty types of edge-modifying devices are distributed as commercial products in Japan; twelve examples are shown in Fig. 1 [2]. Their acoustical efficiencies differ significantly as a result of various thicknesses (i.e., widths in the cross-sectional drawings) and various mechanisms of reducing diffraction. They have been developed through trial-and-error processes using mainly numerical analyses and scale-model experiments to estimate the relationship between the noise-reducing mechanisms and efficiencies.

Road traffic administrators who introduce noise-reducing devices must accurately estimate the efficiency of the devices. The numerical analyses and scale-model experiment including much idealization of the geometrical shapes and boundary conditions of the edge-modifying device do not necessarily provide accurate estimations of the noise-reducing efficiency. It is measurements using a practical product of the edge-modifying device that should provide reliable determinations of noise-reducing efficiency. The efficiency determinations of practical barrier products have been carried out on the basis of ISO 10847 [3] or other equivalent procedures. However, the ISO measurement results are strongly affected by the ground effect and cannot be applied to predict sound propagation in any other terrain. Recently, procedures for determining the efficiency of edge-modifying devices have been proposed by CEN/TS 1793-4 [4]. The CEN/TS is innovative as it excludes reflections from the ground surface and extracts only direct diffraction (i.e., diffracted sound that propagates directly from the edge without being reflected from any other object) by introducing impulse response measurement around the edge. The determined efficiencies are very useful because they are independent of the local terrain of the test facility. However, the CEN/TS or related articles have not yet provided any reasonable basis for the

*e-mail: okubo@kobayasi-riken.or.jp

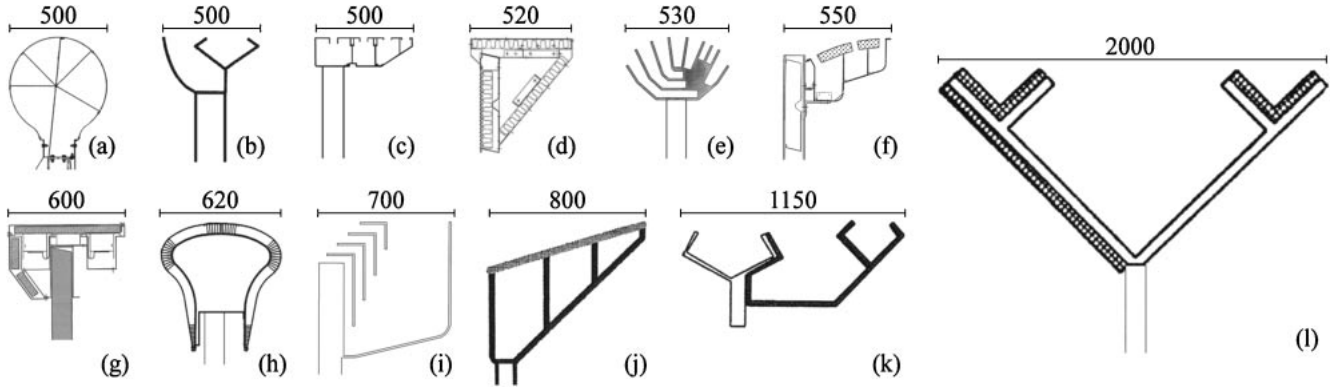

Fig. 1 Examples of edge-modified barriers distributed as commercial products in Japan. Cross-sectional drawings with approximate sizes in mm, sorted in ascending order of the size. Sound sources should be at the left-hand side of the drawings. (a) Absorber with various back cavities. (b) Interference without absorber. (c) Resonators without absorber. (d) Absorbers without back cavity. (e) Interference without absorber. (f) Resonators and absorbers. (g) Active-control systems and absorbers. (h) Absorber without back cavity. (i) Interference without absorber. (j) Absorbers with various back cavities. (k) Interference without absorber. (l) Interference with absorbers.

alignment of the loudspeaker and microphone in their measurement procedures.

The authors have proposed similar procedures for efficiency determination, on the basis of the impulse response measurements [5]. We found that the acoustic efficiency of the edge-modifying device is a function of the angles of the source and receiver, and that the efficiency is almost independent of their radii. On the basis of this finding, a novel procedure for determining the efficiency of the devices has been proposed. The measured efficiency of the device is applicable to the prediction of noise propagation behind edge-modified barriers [6]. In the present paper, the proposed method for the efficiency determination is applied to practical products of edge-modifying devices, and the results are utilized in calculations to predict diffracted noise propagation behind edge-modified barriers.

2. BASIC CONCEPT OF EFFICIENCY DETERMINATION AND PROPAGATION PREDICTION

Figure 2 shows a schematic diagram of a proposed package of efficiency determination and propagation prediction.

In the determination of the acoustical efficiency of edge-modifying devices, the sound pressure level (SPL) difference between the edge-modified barrier and a thick barrier with thickness equivalent to the tested edge-modified barrier is measured as an efficiency index. It should be noted that the barriers for efficiency measurement should be semi-infinite half planes; hence, reflections from the ground or floor of the test facility must be eliminated.

Sound propagation behind an edge-modified barrier is then predicted by adding the determined efficiency index to

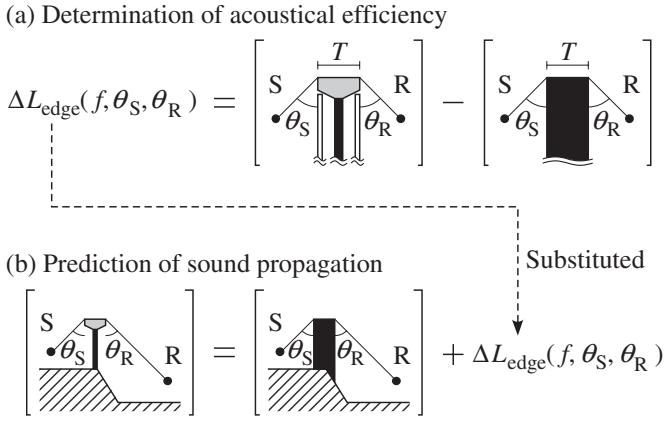

Fig. 2 Framework of the procedures proposed in this paper. Note that S and R denote a point source and a receiver, respectively.

the prediction for a thick barrier. Although the ground effect can be taken into account by using multiple-path method [6], ground effects in the propagation are neglected for simplicity in this paper.

In the previous reports [5,6], both the determination and prediction are normalized with diffraction around a thin simple barrier. In this paper, they are normalized with diffraction around a thick barrier, as shown in Fig. 2; the efficiency index of an edge-modifying device excludes the thickness effect and includes only the effect of the acoustical mechanism on the top surface of the device.

3. DETERMINATION OF ACOUSTICAL EFFICIENCY OF EDGE-MODIFYING DEVICES

3.1. Test Facility

Tested edge-modifying devices are installed on the top of a barrier with a height of around 5 m, as shown in Fig. 3.

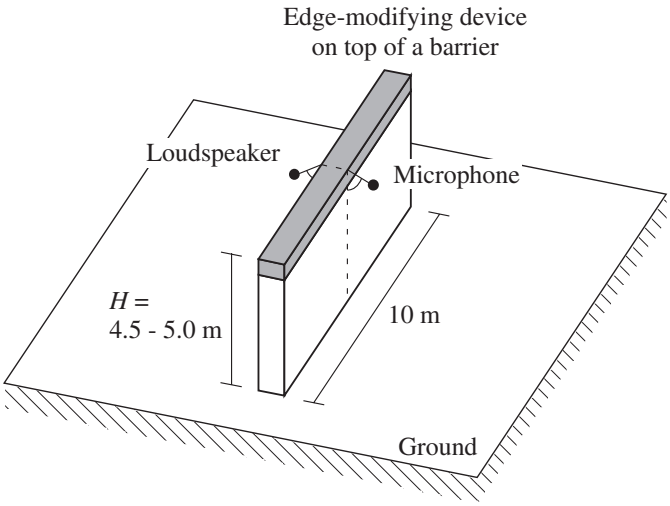

Fig. 3 Overview of the test facility.

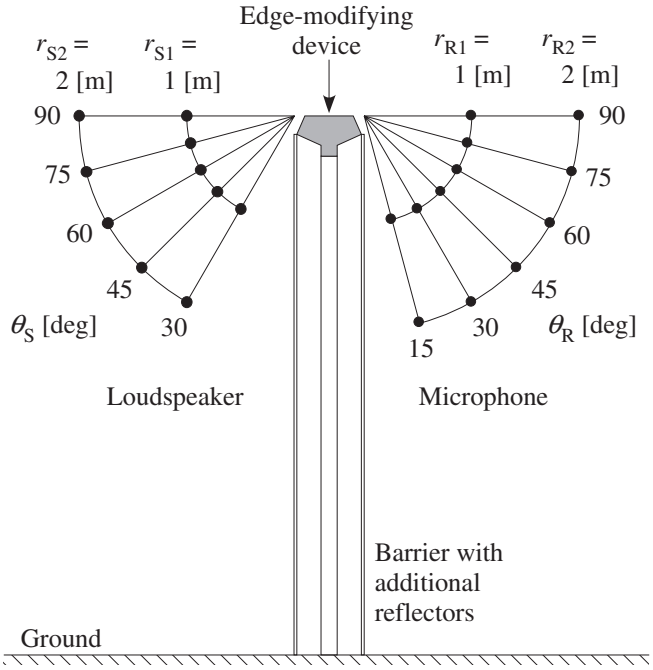

Fig. 4 Positions of loudspeakers and microphones.

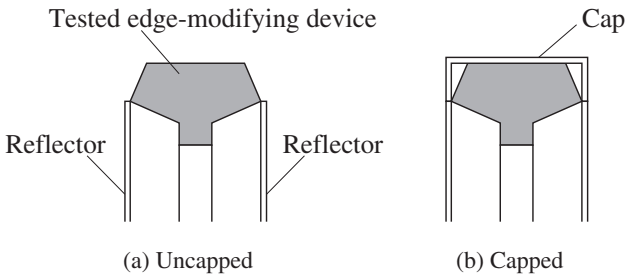

Fig. 5 Definition of uncapped and capped conditions.

Regulations on acoustical characteristics of the ground surface are not necessary because reflections from the ground will be eliminated by the impulse response measurement technique (described later in Section 3.2). The barrier height is set flexibly between 4.5 to 5 meters considering the shape of the tested edge device; the lower limit of 4.5 m is mandatory to eliminate the ground reflection, and the upper limit of 5 m is extendable if measurement work in high place is carried out safely. Diffraction around the side edge will be eliminated similarly by the impulse response measurement, thus a length of 10 m is sufficient for measurement. Loudspeakers and microphones are aligned along circular arcs centered on top of the barrier, as shown in Fig. 4. Their positions are described with radii and angles, where the angle is defined as zero on the surface of the barrier. Measurements will be made for radii of 1 and 2 meters and angles up to 90 degrees at intervals of 15 degrees. The circular arc is set in a plane perpendicular to the barrier edge.

As shown in Fig. 2, the efficiency index is defined as the SPL difference between a barrier with an edge-modifying device and a thick barrier. SPL measurements are repeated under the two conditions shown in Fig. 5: the "uncapped" condition representing a barrier with an edge-modified device and the "capped" condition representing a thick barrier. The straight-wall portion of the test barrier is covered by additional reflective boards. The reflectors can prevent overestimation of the acoustical efficiency of the device; if the reflectors are not introduced, interference due to overhang of the device (not interference due to sound-reducing mechanism on the top surface of the device) greatly decreases sound diffracted behind the barrier [5]. The addition of these reflectors results in a test barrier made of triple panels (i.e., one core barrier between the reflectors) to reinforce transmission loss of the straight-wall portion, compared with the single-panel barrier without the reflectors. Sound transmission through the straight-wall portion, which is harmful to diffraction measurement behind the barrier, is reduced. The core barrier consists of the standard-type barrier panels of NEXCO (Nippon Expressway Company, an expressway company in Japan), which is specified to have transmission losses of more than 25 dB at 400 Hz and more than 30 dB at 1 kHz, with minor modifications. Gaps among the reflectors, the cap and the tested edge device are sealed by narrow wooden strips and adhesive tape.

The test facility is built at an outdoor site, as depicted in Fig. 6. The tested edge-modifying device is mounted at the top of a barrier, and the straight-wall portion is covered by reflectors made of plywood boards. One loudspeaker is moved along an imaginary circular arc, while six microphones are mounted on a circular arc of a steel pipe. The test barrier is surrounded by some buildings and trees. They cause no harm acoustically because reflected sound from

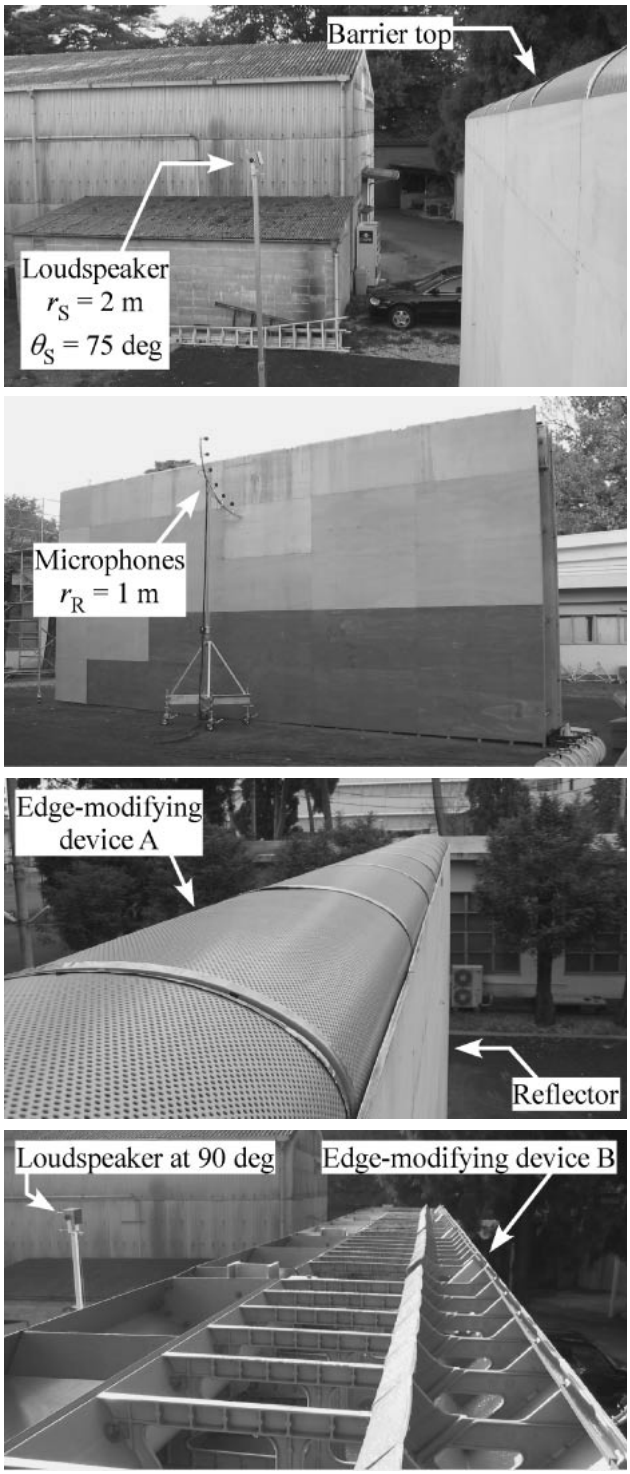

Fig. 6 Appearance of the test facility. (a) View from side edge of the barrier to loudspeaker side. (b) View from microphone side. (c) Close-up view around barrier top with edge-modifying device A. (d) Close-up view around barrier top with edge-modifying device B.

them is eliminated from the impulse response. Rather, the surrounding buildings are beneficial for reducing wind blowing into the test site. Needless to say, building the test barrier in an indoor environment would be the best solution to avoid wind and background noise.

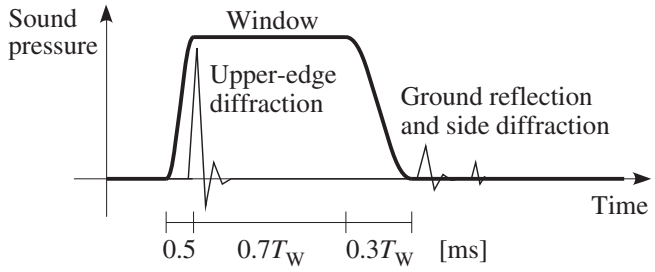

Fig. 7 Schematic diagram of temporal window to extract top-edge diffraction and exclude ground reflection and side diffraction.

3.2. Impulse Response Measurement

Impulse response from a loudspeaker to a microphone is measured using white swept-sine signals [7] with a length of 65536 points at a sampling frequency of 48000 Hz. The measured temporal waveform of the impulse response includes diffraction over the upper edge, followed by reflection from the ground, diffraction around the side edges, and reflection from surrounding buildings and trees. The upper-edge diffraction is extracted using the temporal window shown in Fig. 7. This window is defined on the basis of the Adrienne temporal window specified in CEN/TS [4]. A flat rectangular window of $0.7T_W$ [ms] is set between a leading taper of 0.5 ms and a trailing taper of $0.3T_W$ [ms]. The leading and trailing tapers are defined as half of the Blackman-Harris window. The starting point of the flat window is located at the peak position of the impulse response, with the help of path-length computation. The window length T_W must be defined to exclude both ground reflection and side diffraction. Ground reflection generally reaches the microphone earlier than side diffraction, because the path length of ground reflection is shorter than the path length of side diffraction (see Fig. 3).

The loudspeaker-microphone alignment that provides the earliest ground reflection is the situation where the microphone is set closest to the ground at $r_{R2} = 2$ [m] and $\theta_R = 15$ [deg] (see Fig. 4) for a test barrier with a height of 4.5 meters. In this situation, the difference between edge-microphone path and edge-ground-microphone path is 5.21 meters, corresponding to a 15.3 ms delay. Therefore the window length T_W of 15.3 [ms] is applied to exclude ground reflection; T_W in CEN/TS is set at 10 ms for loudspeaker-microphone geometries around a test barrier with a fixed height of 4 m.

The extracted temporal waveform is converted by FFT to frequency characteristics of SPL. Results in the frequency range corresponding to 1/3 octave bands are summed to approximate the 1/3 octave band SPL. The upper limit of the measurement frequency range is restricted to the 5 kHz band considering a typical road

traffic spectrum, and the lower limit is set at the 100 Hz band considering that the flat window of $0.7T_W = 10.7$ [ms] contains one period of pure tones at 93 Hz for a barrier with a height of 4.5 meters.

In the impulse response measurements, the temporal waveforms of the impulse response are averaged over 10 repetitions to obtain a better signal-to-noise ratio. The SPL decrease in the averaging process owing to the disturbance of air around the barrier edge is investigated in preliminary experiments. The standard deviation among three independent trials of averaging 10 repetitions is less than 0.6 dB below 5 kHz, when the maximum wind speed around the top of the test barrier is 2 m/s or less during the averaging process.

3.3. Definition of Efficiency Index

Impulse response measurements are carried out with source positions described by radii r_{Si} [m] of N_S kinds ($i = 1, 2, \ldots, N_S$) and θ_S [deg], similarly to receiver positions described by radii r_{Rj} [m] of N_R kinds ($j = 1, 2, \ldots, N_R$) and θ_R [deg]. For measurements in this study, $N_S = N_R = 2$, $r_{S1} = r_{R1} = 1.0$ [m] and $r_{S2} = r_{R2} = 2.0$ [m], as shown in Fig. 4. Let $L_{uncap}(f, \theta_S, \theta_R, r_{Si}, r_{Rj})$ [dB] and $L_{cap}(f, \theta_S, \theta_R, r_{Si}, r_{Rj})$ [dB] denote 1/3 octave band SPLs at center frequency f [Hz] for uncapped and capped conditions, respectively. The SPL difference due to removal of the cap $\Delta L_{i,j}(f, \theta_S, \theta_R)$ [dB] is defined as

$$\Delta L_{i,j}(f, \theta_S, \theta_R) = L_{uncap}(f, \theta_S, \theta_R, r_{Si}, r_{Rj}) - L_{cap}(f, \theta_S, \theta_R, r_{Si}, r_{Rj}). \quad (1)$$

Measurements are repeated to obtain $N_S \cdot N_R$ data of $\Delta L_{i,j}(f, \theta_S, \theta_R)$, where $N_S \cdot N_R = 4$ in this study.

On the basis of the previous report [5], the efficiency index of the tested edge-modifying device is defined as a function of frequency, source angle and receiving angle. The arithmetic average of the $N_S \cdot N_R$ values of $\Delta L_{i,j}(f, \theta_S, \theta_R)$ represents the efficiency index $\Delta L_{edge}(f, \theta_S, \theta_R)$ [dB] of the tested edge-modifying device:

$$\Delta L_{edge}(f, \theta_S, \theta_R) = \frac{1}{N_S N_R} \sum_{i=1}^{N_S} \sum_{j=1}^{N_R} \Delta L_{i,j}(f, \theta_S, \theta_R). \quad (2)$$

The definition clearly indicates that $\Delta L_{edge}(f, \theta_S, \theta_R)$ is a negative value when the device reduces diffraction and positive when the device increases diffraction.

4. APPLICATION OF PROPOSED DETERMINATION METHOD TO PRACTICAL PRODUCTS OF EDGE-MODIFYING DEVICES

4.1. Tested Edge-Modifying Devices

Efficiency indices of the three devices shown in Fig. 8 are determined by the procedures described in the previous section. Devices A and B are commercially available products that have already been introduced along actual expressways worldwide (see Figs. 1(h) and (k)), and photographs of them during the efficiency-determination measurements are shown in Figs. 6(c) and (d), respectively. Device C is a prototype product and is currently not for commercial distribution; its photographs are undisclosed because it is still a prototype under development. Devices A and C reduce diffraction because of the absorbing structure of the porous material covered by protective films and perforated panels. Device B reduces diffraction using interference inside a cavity opened upwardly, and does not incorporate any absorbing material. The total height of the test barrier is 5.0 m for devices A and C, and 4.5 m for device B.

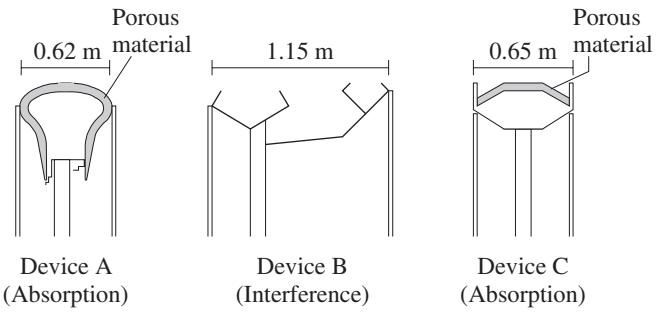

Fig. 8 Cross-sectional view of tested edge-modifying devices.

Figure 8 also shows the arrangement of the additional reflective boards that prevent the overestimation of efficiency. The cap and the reflectors are constructed to form a thick barrier, which has a rectangular cross section equivalent to the maximum height and thickness of the tested edge-modifying device. The reflectors for device A covering the lower half of the absorbing surface, do not decrease the device efficiency; it has been reported that the efficiency of a pressure-release cylindrical edge mainly depends on the upper half of the cylinder and is hardly affected by the lower half [8].

4.2. Measured Impulse Responses

Examples of measured impulse responses are shown in Fig. 9 for the (a) capped and (b) uncapped conditions for Device A measured in the alignment $(\theta_S, \theta_R, r_{Si}, r_{Rj}) = (90, 90, 1, 1)$. In such a shallow-diffraction zone, sound energy outside the extraction window is sufficiently smaller than the energy of upper-edge diffraction inside the window. The fact that the peak in Fig. 9(b) is larger than that in Fig. 9(a) indicates that diffraction increases owing to the removal of the cap in this alignment.

Figures 9(c) and (d) similarly show results in the deepest-diffraction alignment $(\theta_S, \theta_R, r_{Si}, r_{Rj}) = (30, 15, 2, 2)$. Temporal positions of the pressure peaks are later than those in Figs. 9(a) and 9(b) because the radii r_{Si} and r_{Rj} are extended. Ground reflection, side diffraction,

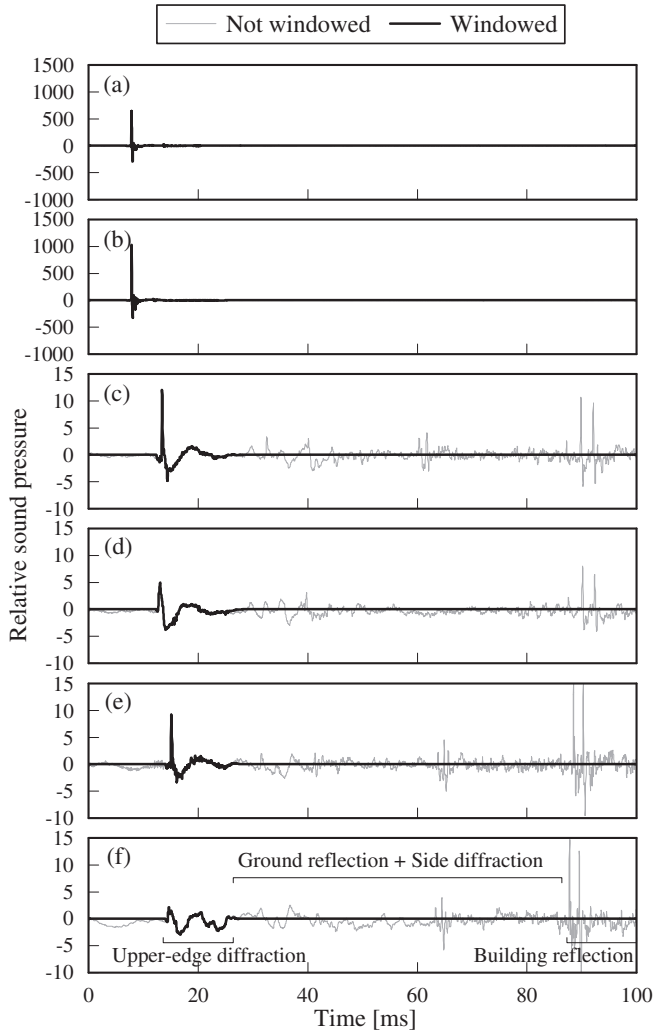

Fig. 9 Examples of measured impulse responses. (a) Device A, capped, $(\theta_S, \theta_R, r_{Si}, r_{Rj}) = (90, 90, 1, 1)$. (b) Device A, uncapped, $(\theta_S, \theta_R, r_{Si}, r_{Rj}) = (90, 90, 1, 1)$. (c) Device A, capped, $(\theta_S, \theta_R, r_{Si}, r_{Rj}) = (30, 15, 2, 2)$. (d) Device A, uncapped, $(\theta_S, \theta_R, r_{Si}, r_{Rj}) = (30, 15, 2, 2)$. (e) Device B, capped, $(\theta_S, \theta_R, r_{Si}, r_{Rj}) = (30, 15, 2, 2)$. (f) Device B, uncapped, $(\theta_S, \theta_R, r_{Si}, r_{Rj}) = (30, 15, 2, 2)$. θ_S and θ_R are in degrees. r_{Si} and r_{Rj} are in meters.

and reflection from buildings surrounding the test facility are no longer negligible compared with upper-edge diffraction, and must be eliminated by the temporal window.

Figures 9(e) and (f) indicate results for device B at the same alignment, $(\theta_S, \theta_R, r_{Si}, r_{Rj}) = (30, 15, 2, 2)$. Temporal positions of the pressure peaks are later than those in Figs. 9(c) and (d) because device B is larger than device A. The waveform of upper-edge diffraction in Fig. 9(f) is longer and more complicated than that in Fig. 9(d) for device A, probably because device B employs interference (or multiple reflections) in cavities. It is not clear whether upper-edge diffraction converges before the end of the window or not; the following analyses are based on the assumption that the length of the temporal window includes sufficient sound energy of upper-edge diffraction.

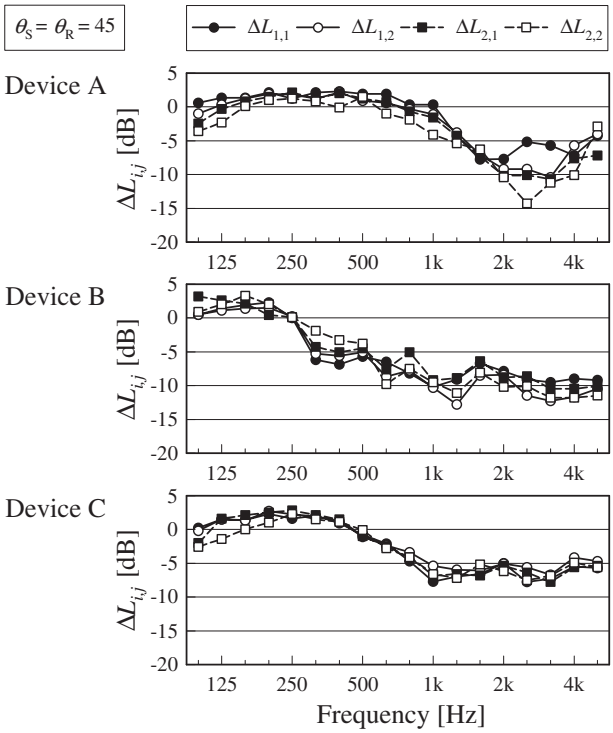

Fig. 10 Dependence of efficiency on radii of source and receiver positions; examples for $\theta_S = \theta_S = 45$ degrees. $\Delta L_{i,j}$ denotes SPL difference due to removal of the cap for combinations of r_{Si} and r_{Rj}.

4.3. Dependence on Radii of Source and Receiver Positions

As mentioned above, the efficiency index is independent of the radii of source and receiver positions. In other words, the SPL difference $\Delta L_{i,j}(f, \theta_S, \theta_R)$ due to removal of the cap should be constant for any combination of radii r_{Si} and r_{Rj}. Frequency characteristics of $\Delta L_{i,j}(f, \theta_S, \theta_R)$ [dB] at $\theta_S = \theta_R = 45$ [deg] are shown in Fig. 10 for different combinations of r_{Si} and r_{Rj}. The dispersion for different radii combinations for device A is large above 2.5 kHz. On the contrary, the dispersion for device C is obviously small. Here, results for only $\theta_S = \theta_R = 45$ are shown, and a similar tendency is observed with other angles.

The assumption that the efficiency is independent of the radii is based on a distribution of wavefronts behind barriers shown in Fig. 11(a). These equiphase contours are calculated using an analytical solution on a diffracted sound field behind a semi-infinite half plane [9]. The wavefronts in the shadow region form concentric circles focused on the barrier edge. Similar wavefronts appear behind edge-modified barriers if their shoulders (i.e., upper two corners of the device in cross-sectional drawings) are squarely angulated, as shown in Fig. 11(b), such as in device C. Hypothetical focuses of diffracted fields behind

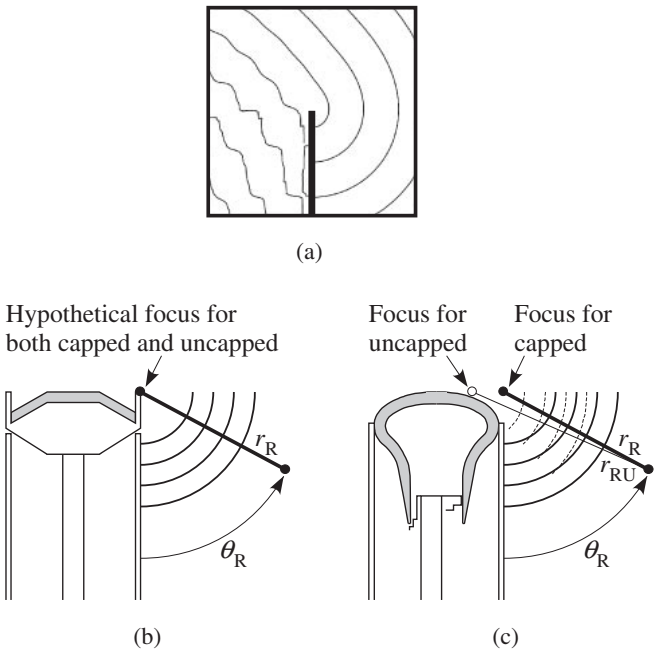

Fig. 11 Wavefronts and imaginary focus for diffracted sound field around barriers. (a) Analytical solution [9] of diffraction around a thin barrier, (b) schematic diagram for edge-modified barriers with rectangular shoulders, and (c) schematic diagram for edge-modified barriers with rounded shoulders.

capped and uncapped barriers are identical, and the assumption of radius independence stays true. On the contrary, for device A or B with rounded shoulders, as shown in Fig. 11(c), the hypothetical focuses are not identical between capped and uncapped conditions. For these devices, the radius-independence assumption is no longer appropriate because of a double definition of radii: the original definition r_R centered on the cap shoulder and another definition r_{RU} centered on the hypothetical focus for the uncapped condition. When one endeavors to determine the efficiencies of edge-modifying devices with rounded shoulders, such as device A or B, dispersion due to the radius combination is inevitable. The most important goal of the present study is efficiency measurement excluding the ground effect, and measurements for long radii are cost-consuming or unrealistic because a much higher test barrier is required to exclude ground reflection. Therefore, the radius-dependence measurement is not introduced, and the efficiency is determined on the assumption that SPL reduction due to the device, averaged for multiple combinations of source radii and receiver radii using Eq. (2), should approximate the expected value of reduction of diffracted sound in the far field.

4.4. Results of Efficiency Determination

Determined efficiency indices $\Delta L_{edge}(f, \theta_S, \theta_R)$ for devices A, B and C are shown in Fig. 12 as frequency characteristics of SPL reduction for each combination of θ_S and θ_R. Efficiencies for $\theta_S = 75$ and 45 are measured but results are omitted to save space. Negative values of $\Delta L_{edge}(f, \theta_S, \theta_R)$ indicate that the diffraction is reduced.

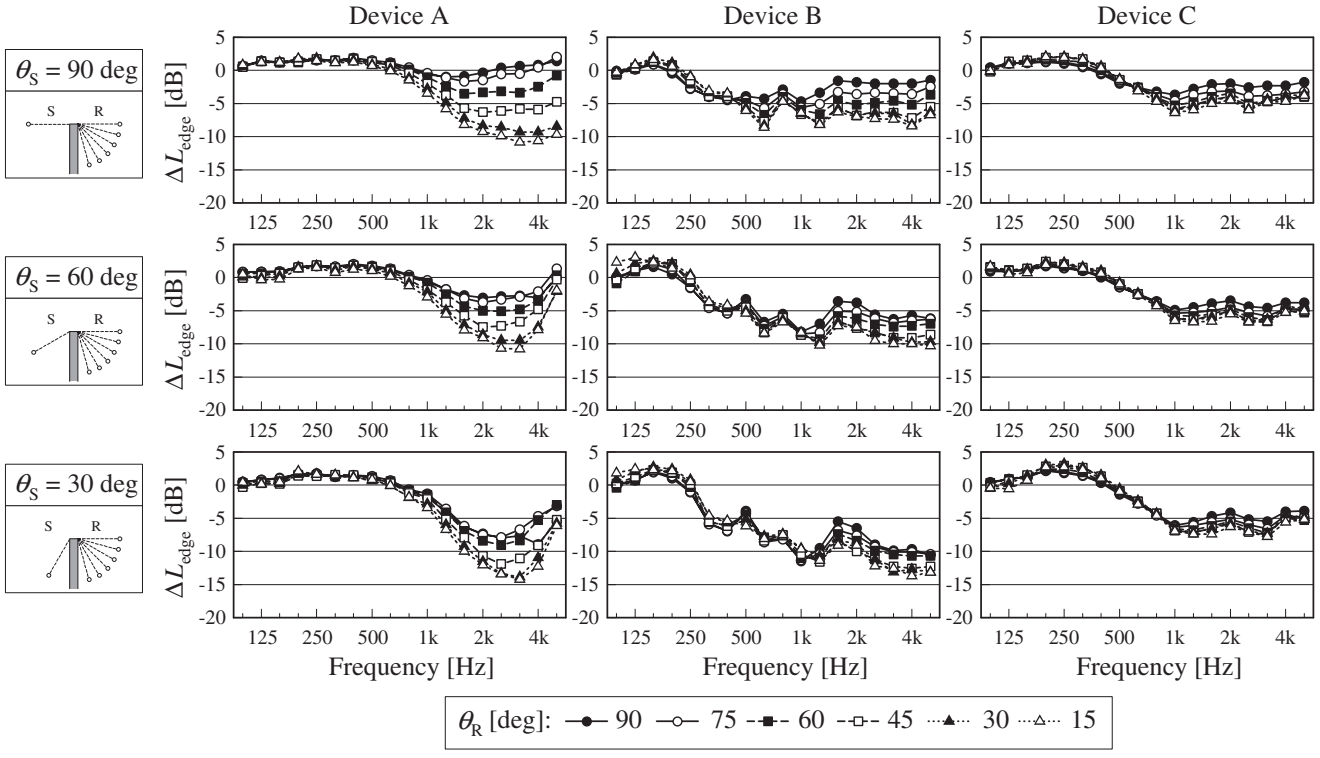

Fig. 12 Determined efficiency indices $\Delta L_{edge}(f, \theta_S, \theta_R)$ [dB] of devices A, B and C.

The closer the source or the receiver approaches the barrier surface (i.e., θ_S or θ_R becomes smaller), the more efficiently the device reduces diffraction. This corresponds to conventional qualitative knowledge. The efficiency index of around 2.5 kHz for device A is drastically affected by θ_S and θ_R, while that of between 500 Hz to 1 kHz for device B is almost independent of θ_R for small θ_S.

Frequency characteristics of the efficiency depend on acoustical mechanisms such as absorption or interference to reduce diffraction. Devices A and C are efficient in the high-frequency range where the absorbing materials are efficient. Although they introduce an identical absorbing structure, efficiency indices for devices A and C differ slightly; the efficiency index for device A reaches a minimum at 2.5 kHz, but that for device C is almost constant above 1 kHz. This indicates that the efficiency of an absorber-type device depends on not only the structure of the absorber but also the external shape of the device. Device B is efficient in a lower frequency range than the other devices.

For all devices, efficiency indices in the low-frequency range are positive, that is, the devices may cause an increase of diffraction. The indices are, however, defined with reference to a thick barrier. The positive indices and thickness effect will cancel each other out in the low-frequency range, and the whole effect of the device compared with a simple barrier may be around zero.

5. PREDICTION OF NOISE PROPAGATION USING DETERMINED EFFICIENCY INDICES

The measured efficiency indices described in the previous section are utilized to predict the diffracted sound field behind edge-modified noise barriers.

5.1. Calculation Method

An edge-modified noise barrier between a point source and a receiver is supposed, as shown in Fig. 13(a). The cross-sectional shape of this terrain infinitely continues along the z-axis direction. For simplicity, the ground on the receiver-side does not exist and hence ground reflection is neglected. The point source is placed on the reflective flat ground surface to avoid interference due to ground reflection. The straight-wall portion of the edge-modified barrier is reflective.

First, the prediction method for a simple barrier is considered. SPL behind a simple barrier $L_{SB}(f)$ [dB] against a point source with sound power level $L_W(f)$ [dB] at frequency f[Hz] is defined as

$$L_{SB}(f) = L_W(f) - 8 - 20\log r + \Delta L_{dif,sd}(f), \qquad (3)$$

where r [m] denotes the distance along the direct path. $\Delta L_{dif,sd}(f)$ [dB] denotes a correction term for diffraction around a simple barrier, and is defined as

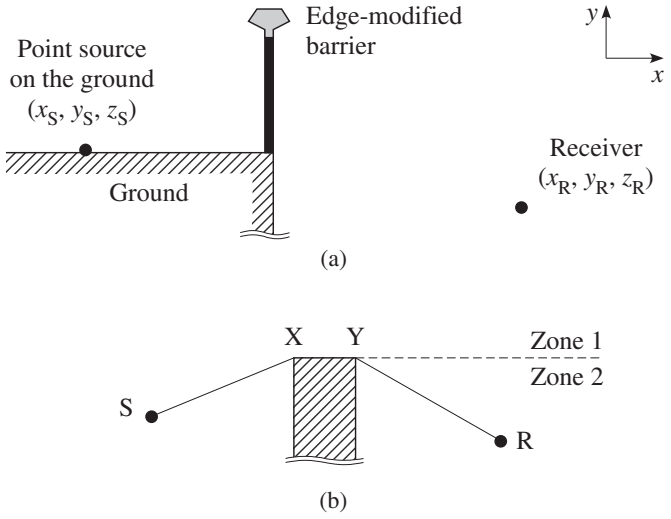

Fig. 13 Prediction of diffraction behind edge-modified barriers. (a) Cross section of the sound field considered in the prediction. (b) Schematic diagram for double diffraction around a thick barrier.

$$\Delta L_{dif,sd}(f) = \Delta L_{dif}(2f\delta/c), \qquad (4)$$

where δ [m] is the difference in length between direct and diffracted paths, and c [m/s] is the speed of sound. $\Delta L_{dif}(N)$ [dB] denotes the insertion loss of a reflective semi-infinite barrier, and is defined as a function of the Fresnel number $N = 2f\delta/c$:

$$\Delta L_{dif}(N) = \begin{cases} -13 - 10\log N & \text{for } 1 \le N \\ -6 - 7\sqrt{N} & \text{for } 0 \le N < 1 \\ -6 + 12\sqrt{-N} & \text{for } -0.25 \le N < 0 \\ 0 & \text{for } N < -0.25 \end{cases}. \qquad (5)$$

This equation is a slight modification of a mathematical expression of Maekawa's empirical chart [10].

SPL behind an edge-modified barrier is similarly defined. Considering a correction term for diffraction around a thick barrier $\Delta L_{dif,dd}(f)$ [dB] and the determined efficiency index $\Delta L_{edge}(f, \theta_S, \theta_R)$ [dB], SPL behind the edge-modified barrier $L_{EMB}(f)$ [dB] is defined as

$$L_{EMB}(f) = L_W(f) - 8 - 20\log r + \Delta L_{dif,dd}(f) + \Delta L_{edge}(f, \theta_S, \theta_R). \qquad (6)$$

$\Delta L_{dif,dd}(f)$ is calculated as double diffraction [11] shown in Fig. 13(b):

$$\Delta L_{dif,dd}(f) = \begin{cases} \Delta L_{dif}(N_{SXR}) & \text{for Zone 1} \\ \Delta L_{dif}(N_{SXR}) + \Delta L_{dif}(N_{XYR}) + 6 & \text{for Zone 2, } N_{SXR} \ge N_{SYR} \\ \Delta L_{dif}(N_{SXY}) + \Delta L_{dif}(N_{SYR}) + 6 & \text{for Zone 2, } N_{SXR} < N_{SYR} \end{cases} \qquad (7)$$

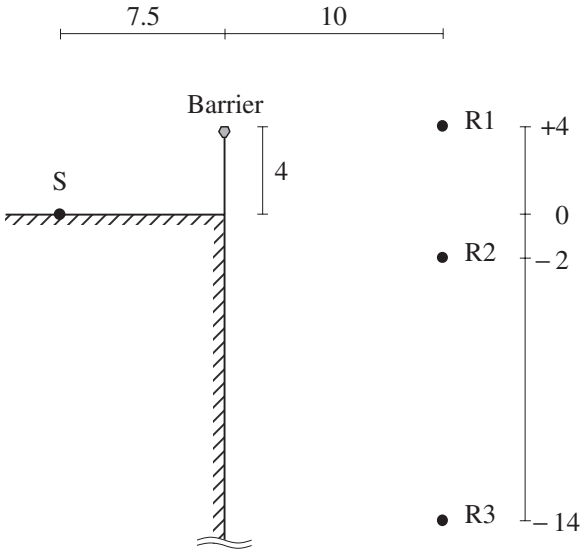

Fig. 14 Geometry for accuracy validation.

$\Delta L_{\mathrm{edge}}(f, \theta_{\mathrm{S}}, \theta_{\mathrm{R}})$ has been measured only for discrete angles of θ_{S} and θ_{R}. Values of $\Delta L_{\mathrm{edge}}(f, \theta_{\mathrm{S}}, \theta_{\mathrm{R}})$ for intermediate θ_{S} or θ_{R} to assure continuity of Eq. (6) are obtained by linear interpolation between measured data.

5.2. Validation of Prediction Accuracy

The accuracy of the prediction is validated in the situation shown in Fig. 14. A point source and a receiver are set in the same plane perpendicular to the barrier edge, i.e., $z_{\mathrm{S}} = z_{\mathrm{R}}$. Predictions are carried out for four barriers: a simple barrier without an edge-modifying device and three edge-modified barriers with devices A, B and C. The barriers have a constant height of 4 meters including the devices. $L_W(f)$ is defined as a typical A-weighted power spectrum of a running vehicle [12], and A-weighted SPLs behind a simple barrier and edge-modified barriers are calculated using Eqs. (3) and (6), respectively. Note that the results of the calculation correspond to maximum A-weighted SPLs during a single vehicle passage, not L_{AE} (A-weighted sound exposure level) integrated for the entirety of a single vehicle passage, nor L_{Aeq} (equivalent continuous A-weighted sound pressure level) for traffic flow of multiple vehicle passages.

Predictions are compared with the results of two-dimensional boundary element method (2-D BEM) analyses for the validation of accuracy. Insertion losses due to both barriers and terrain are calculated by 2-D BEM, with absorbing boundaries parameterized simply as impedance boundaries on the locally-reacting hypothesis. Normal-incidence acoustic impedances of core samples of absorbing materials introduced in devices A and C are measured using the two-microphone method in the impedance tube [13]. The frequency range is limited to below 2.5 kHz because of the computational costs of 2-D BEM.

Comparisons of the results of the proposed method and 2-D BEM are shown in Fig. 15 as frequency characteristics of A-weighted SPL. Predictions by the proposed method for the simple barrier and the barrier with device B agree well with those by 2-D BEM. The difference in results for device B between the proposed method and 2-D BEM may mainly depend on the idealization of the boundary shape of the edge device B. In 2-D BEM, the device B is idealized as a completely two-dimensional shape, and sound penetration between interference cavities through partitioning panels is excluded by adopting an infinite transmission loss and no aperture in the partitions. Conversely, the actual product of device B consists of three-dimensional parts, as shown in Fig. 6(d), and sound penetration between cavities through thin metal and polycarbonate partitions and through small gaps designed to drain rain and dust cannot be neglected. Disagreement between the results of 2-D BEM and the proposed method may be caused by the finite transmission loss of the partitions in the low-frequency range, and by the three-dimensional parts and the gaps in the high-frequency range.

For the barriers with devices A and C, SPLs predicted by proposed method are larger than that predicted by 2-D BEM in the high-frequency range. The difference may be due to the overestimation of absorption in 2-D BEM with the simple locally-reacting hypothesis concerning absorbing materials [14]. As shown in Fig. 16, the sound path incoming to device A makes a grazing angle incidence to the absorbing surface, and the locally-reacting hypothesis collapses with the grazing-angle incidence. For device C, SPL difference in Fig. 15 owing to the underestimation in 2-D BEM is smaller compared with device A, because the incidence angle is far from the grazing angle around the shoulders of the device. In summary, the SPL differences between the proposed method and 2-D BEM in Fig. 15 do not necessarily imply that the proposed method is inaccurate. The difference due to the overestimation of absorption does not appear for device B because no absorbing material is included in the device.

6. EFFICIENCY OF EDGE-MODIFYING DEVICES ABOVE BARRIERS

Efficiency indices have been determined in a restricted range of angles for $\theta_{\mathrm{S}} \leq 90$ [deg] and $\theta_{\mathrm{R}} \leq 90$ [deg]. Sometimes predictions for $\theta_{\mathrm{R}} > 90$ are required in practical situations for high-rise buildings. In this chapter, efficiency determination and propagation prediction for $\theta_{\mathrm{R}} > 90$ are discussed.

6.1. Estimation of Efficiency above Barrier Height by Extrapolation

On the basis of Fig. 11(a) or Huygens's principle, wavefronts around an edge-modified barrier can be

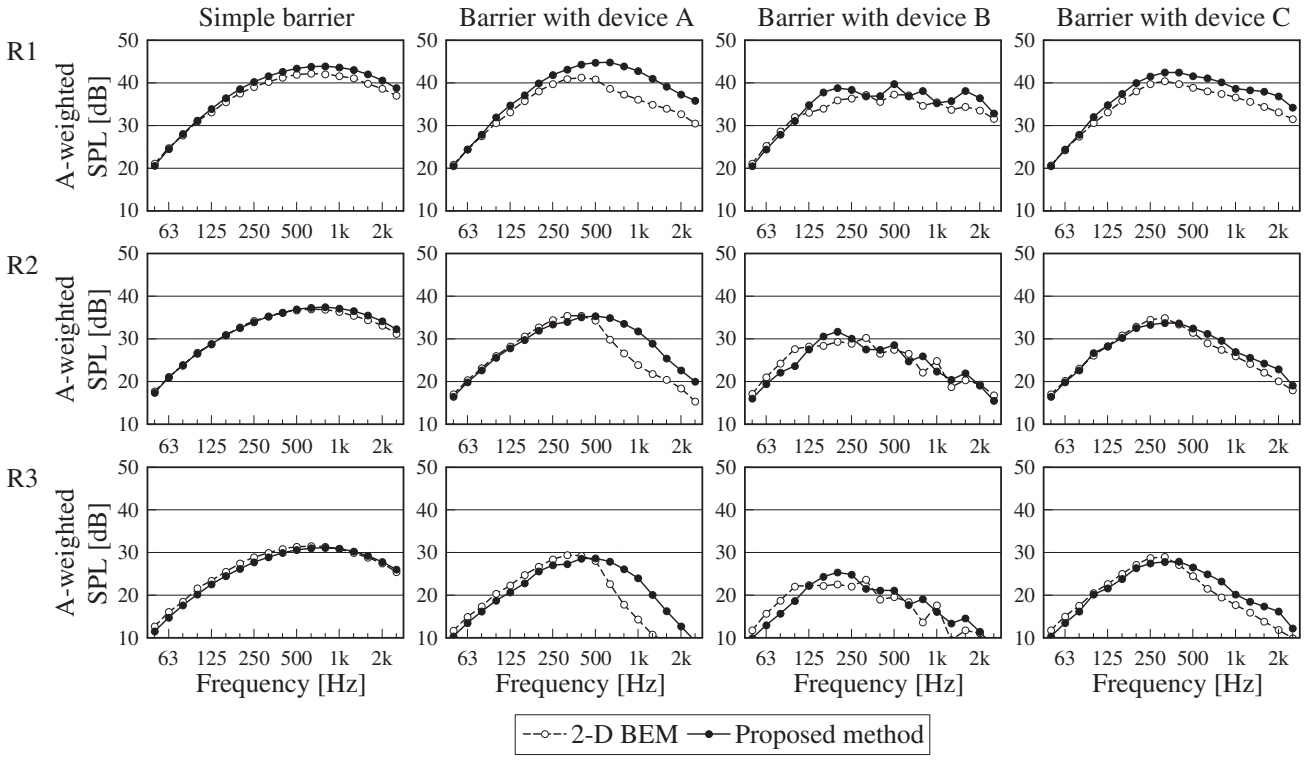

Fig. 15 Prediction of diffraction using proposed method for a simple barrier and barriers with devices A, B and C, compared with 2-D BEM analyses.

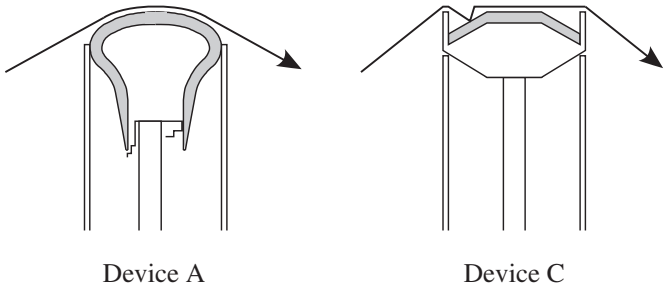

Fig. 16 Sound incidence on absorbing surfaces of devices A and C.

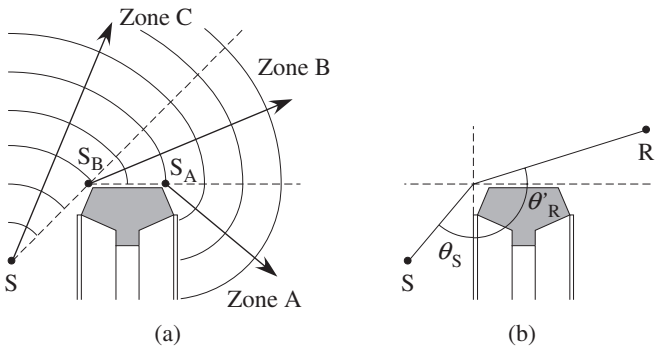

Fig. 17 Efficiency of edge-modifying devices above barriers. (a) Schematic diagram for wavefronts around an edge-modified barrier: S_A denotes a receiver-side top edge which diffraction in Zone A is related to, and S_B denotes a source-side top edge which diffraction in Zone B is related to. (b) Definition of angle θ'_R for efficiency estimation.

depicted as in Fig. 17(a). The determination procedure in zone A has already been established. In zone C, the efficiencies of devices must be quite small because direct sound from the source is more dominant than diffracted sound, and the efficiency index may be unworthy of measurement.

In the intermediate zone B, wavefronts should travel radially from a hypothetical focus at S_B. If one tries to determine the efficiency index in this zone, measurements must be carried out along new circular arcs centered on S_B instead of the extension of arcs centered on S_A in Fig. 4. Efficiency measurements with microphones set above 7 meters are not useful from the viewpoint of cost-effectiveness and safety in measurement operation. Now we propose the estimation of efficiency in the zones B and C by extrapolating the efficiency index measured in zone A.

Let θ'_R [deg] denote the receiving angle centered on S_B, as shown in Fig. 17(b). On the assumption that the efficiency is zero in zone C and that the efficiency in zone B can be interpolated linearly between zones A and C, efficiency index $\Delta\hat{L}_{\mathrm{edge}}(f, \theta_S, \theta'_R)$ [dB] is estimated as

$$\Delta\hat{L}_{\mathrm{edge}}(f, \theta_S, \theta'_R) = \begin{cases} \Delta L_{\mathrm{edge}}(f, \theta_S, 90) \cdot \dfrac{\theta_S + \theta'_R - 180}{\theta_S - 90} & \\ \qquad \text{for } 90 < \theta'_R < 180 - \theta_S \\ 0 \qquad \text{for } 180 - \theta_S \le \theta'_R \end{cases} \tag{8}$$

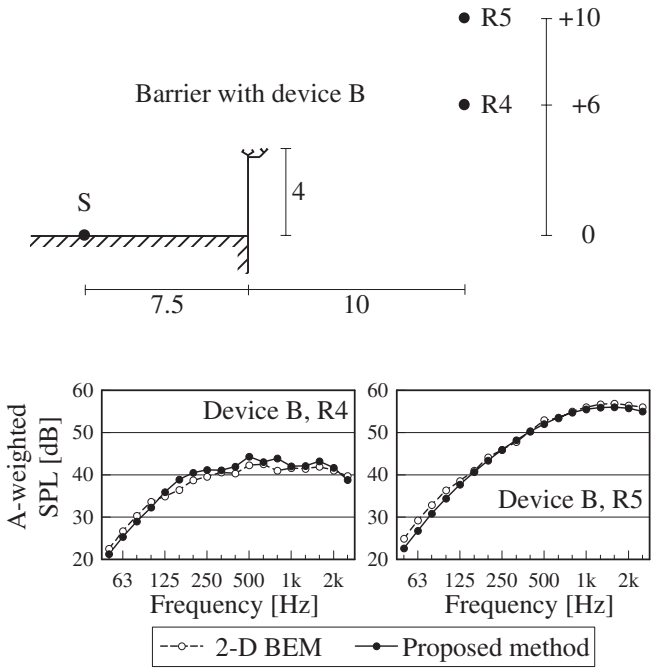

Fig. 18 Prediction of diffraction above barrier top using estimated efficiency for device B, compared with results of 2-D BEM analyses.

6.2. Propagation Prediction Using Estimated Efficiency

Propagation above the barrier height is predicted using Eqs. (6) and (8) for the barrier with device B. Results are shown in Fig. 18; receivers R4 and R5 are in zones B and C, respectively. The proposed method is almost as precise as 2-D BEM, thus Eq. (8) provides a sufficiently accurate estimation for practical predictions. The predicted SPL distribution should be continuous throughout all zones A, B and C, because both Eqs. (6) and (8) are continuous.

7. CONCLUSIONS

The procedures of efficiency determination for edge-modifying devices were applied to practical products, and the results were utilized to predict diffraction behind edge-modified noise barriers. The accuracy of the prediction by the proposed method was validated, which also led to the validation of the reasonableness of the efficiency determination procedure. The ground effect on the receiving side, which is neglected in this paper, can be considered using the multiple-path method [6]. The proposed prediction method becomes applicable not only for road traffic noise, but also for any sound source by substituting the appropriate power spectrum for $L_W(f)$.

In this study, the prediction was restricted to a plane perpendicular to the barrier edge, i.e., $z_S = z_R$ in Fig. 13, because the efficiencies of the devices were measured in only for $z_S = z_R$. Prediction with $z_S \neq z_R$ is necessary to predict L_{Aeq} due to road traffic noise. The applicability of the efficiency measured with $z_S = z_R$ to the prediction with $z_S \neq z_R$ is investigated [15]. Predictions by the proposed method with modifications for $z_S \neq z_R$ have been compared with on-site measurements for road traffic noise behind edge-modified barriers along actual expressways [16].

ACKNOWLEDGEMENTS

The authors thank Nitto Boseki Co. Ltd., Bridgestone Corporation, and Nippon Steel & Sumikin Metal Products Co. Ltd. for providing edge-modifying device products and permitting us to disclose the results of efficiency determination.

REFERENCES

[1] K. Fujiwara and K. Ono, "Sound diffraction by a barrier with cylindrical edge," *Proc. Meet. INCE Jpn.*, pp. 153–156 (1976) (in Japanese).

[2] T. Okubo, "Edge-modified noise barriers," *J. INCE Jpn.*, **28**, 317–322 (2004) (in Japanese).

[3] ISO 10847:1997, *Acoustics — in situ determination of insertion loss of outdoor noise barriers of all types* (International Organization for Standardization, Geneva, Switzerland, 1997).

[4] CEN/TS 1793-4:2003, *Road traffic noise reducing devices — Test method for determining the acoustic performance — Part 4: Intrinsic characteristics – In situ values of sound diffraction* (European Committee for Standardization, Brussels, Belgium, 2003).

[5] T. Okubo and K. Yamamoto, "Procedures for determining the acoustic efficiency of edge-modified noise barriers," *Appl. Acoust.*, **68**, 797–819 (2007).

[6] T. Okubo and K. Yamamoto, "Simple prediction method for sound propagation behind edge-modified barriers," *Acoust. Sci. & Tech.*, **28**, 7–15 (2007).

[7] Y. Suzuki, F. Asano, H. Y. Kim and T. Sone, "An optimum computer-generated pulse signal suitable for the measurement of very long impulse responses," *J. Acoust. Soc. Am.*, **97**, 1119–1123 (1995).

[8] T. Okubo and K. Fujiwara, "Efficiency of a noise barrier with an acoustically soft cylindrical edge for practical use," *J. Acoust. Soc. Am.*, **105**, 3326–3335 (1999).

[9] J. J. Bowman, T. B. Senior and P. L. E. Uslenghi, *Electromagnetic and Acoustic Scattering by Simple Shapes* (North-Holland Publishing, Amsterdam, 1969).

[10] K. Yamamoto and K. Takagi, "Expressions of Maekawa's chart for computation," *Appl. Acoust.*, **37**, 75–82 (1992).

[11] K. Takagi, "Some remarks on practical methods for calculating acoustical diffraction," *Appl. Acoust.*, **31**, 119–132 (1990).

[12] S. Kono, Y. Oshino, T. Iwase, T. Sone and H. Tachibana, "Road traffic noise prediction model 'ASJ RTN-model 2003' proposed by the Acoustical Society of Japan — Part 2: Calculation model of sound emission or road vehicles," *Proc. 18th Int. Congr. Acoust.*, IV-2793-2796 (2004).

[13] J. Y. Chung and D. A. Blaser, "Transfer function method of measuring in-duct acoustic properties. I. Theory," *J. Acoust. Soc. Am.*, **68**, 907–913 (1980).

[14] T. Ishizuka and T. Okubo, "Inaccuracy due to local-reaction model in numerical analyses for noise-shielding efficiency of barriers with absorbing edge," *Acoust. Sci. & Tech.*, **30**, 372–375 (2009).

[15] T. Okubo, K. Yamamoto, O. Funahashi and M. Yamamoto,

"Barriers against road traffic noise: relationship between L_{Aeq} reduction at roadside and $L_{p\mathrm{A}}$ reduction determined in normal-incidence alignment," *Proc. inter-noise 2008*, No. 0182 (2008).

[16] T. Okubo, T. Matsumoto, K. Yamamoto, O. Funahashi, T. Okura, K. Nakasaki and M. Yamamoto, "Noise barriers with diffraction-reducing devices on top edge: Propagation prediction applying intrinsic efficiencies determined by impulse-response measurement," *Proc. inter-noise 2009*, in09_435 (2009).